Supporting Information for "Seismic evidence for a change in the large scale tomographic pattern across the D" layer"

S. Durand,[1,2] Eric Debayle,[1] Y. Ricard,[1] and S. Lambotte[3]

Corresponding author: S. Durand, Institut für Geophysik, Corrensstr. 24, 48149 Münster, Deutschland (durand@uni-muenster.de)

[1]Laboratoire de Géologie de Lyon - Terre, Planètes, Environnement, CNRS, UMR 5276, École Normale Supérieure de Lyon, Université de Lyon, Université Claude Bernard Lyon 1, 2 rue Raphaël Dubois, Bâtiment Géode 69622 Villeurbanne Cedex, France

[2]Institut für Geophysik, Corrensstr. 24, 48149 Münster, Deutschland

[3]Institut de Physique du Globe de Strasbourg, UMR 7516, Université de Strasbourg, EOST/CNRS, Strasbourg, France

Contents of this file

1. Figures S1 to S5

2. Tables S1 to S5

Introduction

This supporting information provides 5 figures and 5 tables.

Figure S1 is the same as Figure 1 in the paper except that tomographic models (SEMUCB-WM1 [*French & Romanowicz*, 2014], S362WMANI+M [*Moulik & Ekström*, 2014] and SP12RTS [*Koelemeijer et al.*, 2016]) have not been filtered out of the spherical harmonic degrees greater than 8.

Figure S2 displays the results of an inversion of the same normal mode data as in S40RTS, including only low branches (n $<$ 6) self-coupling normal modes. We present the results in the same way as in Figure 2 of the paper. We separate the even and odd parts and also show the sum of the two for the model obtained from this test, and for the other tomographic models (SEMUCB-WM1 [*French & Romanowicz*, 2014], S362WMANI+M [*Moulik & Ekström*, 2014], S40RTS [*Ritsema et al.*, 2011]). Figure S2 demonstrates that when using the same data as in previous studies, we retrieve a strong degree 2 with no major change across the D" layer.

Figure S3 displays the results of the tests done with different (α,β) and (ρ,β) scaling laws. We present the same kind of plots as in Figure 3 of the paper for each test. Test1 refers to the scaling used in S40RTS [*Ritsema et al.*, 2011] and Test2 to that deduced from SP12RTS [*Koelemeijer et al.*, 2016]. Figure S3 shows that whatever the scaling, stronger

odd degrees are found near the CMB with a degree 3 that becomes as large as degree 2. We also agree with SP12RTS on a weaker degree 2 at the base of the mantle compared to other previous models.

Figure S4 displays the amplitude of the spherical harmonic degree 2 at the base of the mantle for various inversions depending on which data constrain the velocity structure at the base of the mantle: body wave data only (as in SEMUCB-WM1 [*French & Romanowicz*, 2014]), normal modes only (as in SEISGLOB1 and in two tests done with other (α,β) and (ρ,β) scaling laws) and a combination of normal modes and body waves (as in SP12RTS [*Koelemeijer et al.*, 2016]). Normal modes do not require the strong degree 2 suggested by body wave observations. We speculate that the interpretation of body waves degree 2 might be affected by their uneven sampling of the mantle, or by anisotropy in the deepest mantle.

Figure S5 displays some observed cross-coupling splitting functions measured by *Deuss et al.* [2013] (2nd column) compared to the predictions computed in the tomographic model S20RTS [*Ritsema et al.*, 2004] (3rd column) and in SEISGLOB1 (4th column). In the first column are also plotted the corresponding normalized shear velocity kernels computed in model PREM [*Dziewonski & Anderson*, 1981]. We display the same observations as in figure 9 of *Deuss et al.* [2013] and find exactly the same predictions, proving that our numerical code works perfectly well.

Tables S1 and S2 summarize the normal modes that have been included in the inversion. Table S1 lists the selected modes for the self-coupling coefficients and Table S2 the selected

modes for the cross-coupling coefficients. They all come from a compilation of various published data from which we excluded the inner core sensitive modes.

Table S3 provides a description of the tomograohic models used in the study for comparison.

Table S4 is the same as that provided in Figure 4 but we added the misfit obtained for the results of the tests done with the other scaling laws (Test1 refers to the scaling used in S40RTS[*Ritsema et al.*, 2011] and Test2 to that deduced from SP12RTS [*Koelemeijer et al.*, 2016]). Whatever the scalings, the misfits are very similar except for the Stoneley mode ${}_1S_{13}$ for which the obtained misfit is significantly larger in the two tests.

Table S5 displays the data misfits obtained for SEISGLOB1, the results of the two tests done with other scaling laws (Test1 refers to the scaling used in S40RTS[*Ritsema et al.*, 2011] and Test2 to the one deduced from SP12RTS [*Koelemeijer et al.*, 2016]) and the other recent tomographic models (SEMUCB-WM1 [*French & Romanowicz*, 2014], S362WMANI+M [*Moulik & Ekström*, 2014] and SP12RTS [*Koelemeijer et al.*, 2016]). SEISGLOB1 or the results of the tests better explain the normal mode data that have been included compared to the other models.

References

Deuss, A., Ritsema, J., van Heijst, H., 2013, A new catalog of normal-mode splitting function measurements up to 10mHz , *Geophys. J. Int.*, **193**, 920–937.

Dziewonski, A. M., Anderson, D. l., 1981, Preliminary reference Earth model, *Phys. Earth. Planet. Inter.*, **25**, 297–236.

French, S.W., Romanowicz, B., 2014, Whole-mantle radially anisotropic shear-velocity structure from spectral-element waveform tomography, *Geophys. J. Int.*, **199**, 1,303–1,327.

Koelemeijer, P.J., Ritsema, J.,Deuss, A., van Heijst, H-J., 2016, SP12RTS: a degree-12 model of shear- and compressional-wave velocity for Earth's mantle, *Geophys. J. Int.*, **204**, 1,024–1,039.

Moulik, P., Ekström, G., 2014, An anisotropic shear velocity model of the Earth's mantle using normal modes, body waves, surface waves and long-period waveforms, *Geophys. J. Int.*, **199**(3), 1,713–1,738.

Ritsema, J., van Heijst, H., Woodhouse, J.H., 2004, Global transition zone tomography, *J. Geophys. Res.*, **109**, B02302, doi:10.1029/2003JB002610.

Ritsema, J., Deuss, A., van Heijst, H.J., Woodhouse, J.H., 2011, S40RTS: a degree-40 shear-velocity model for the mantle from new Rayleigh wave dispersion, teleseismic traveltime and normal-mode splitting function measurements, *Geophys. J. Int.*, **184**, 1,223–1,236.

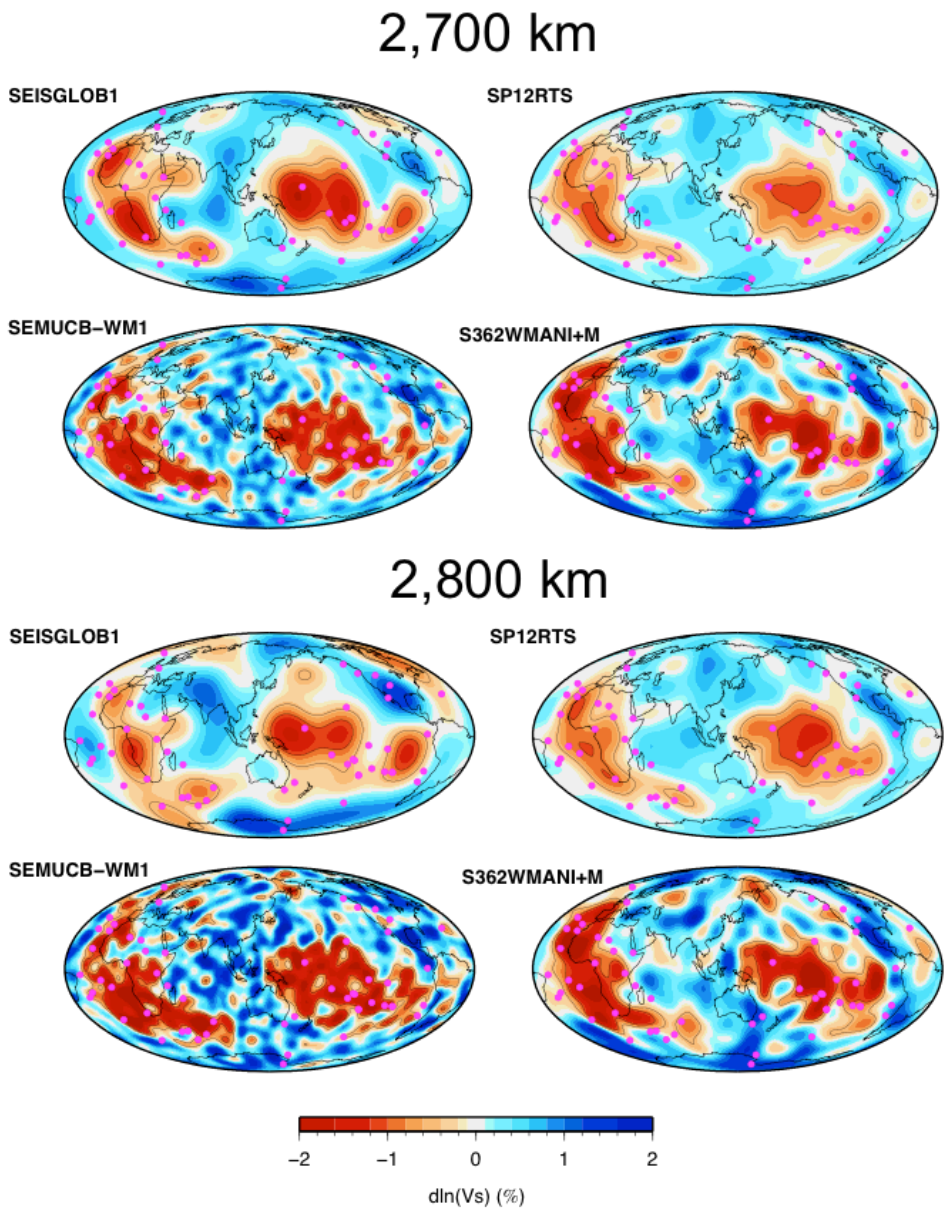

Figure 1. Shear velocity heterogeneities in SEISGLOB1 and three recent tomographic models (SEMUCB-WM1 [*French & Romanowicz*, 2014], S362WMANI+M [*Moulik & Ekström*, 2014], SP12RTS [*Koelemeijer et al.*, 2016]) at 2,700 (top) and 2,800 (bottom) km depth. We also plot the contour lines at -0.50% and -1%. The color scale is in percent with respect to model PREM [*Dziewonski & Anderson*, 1981].

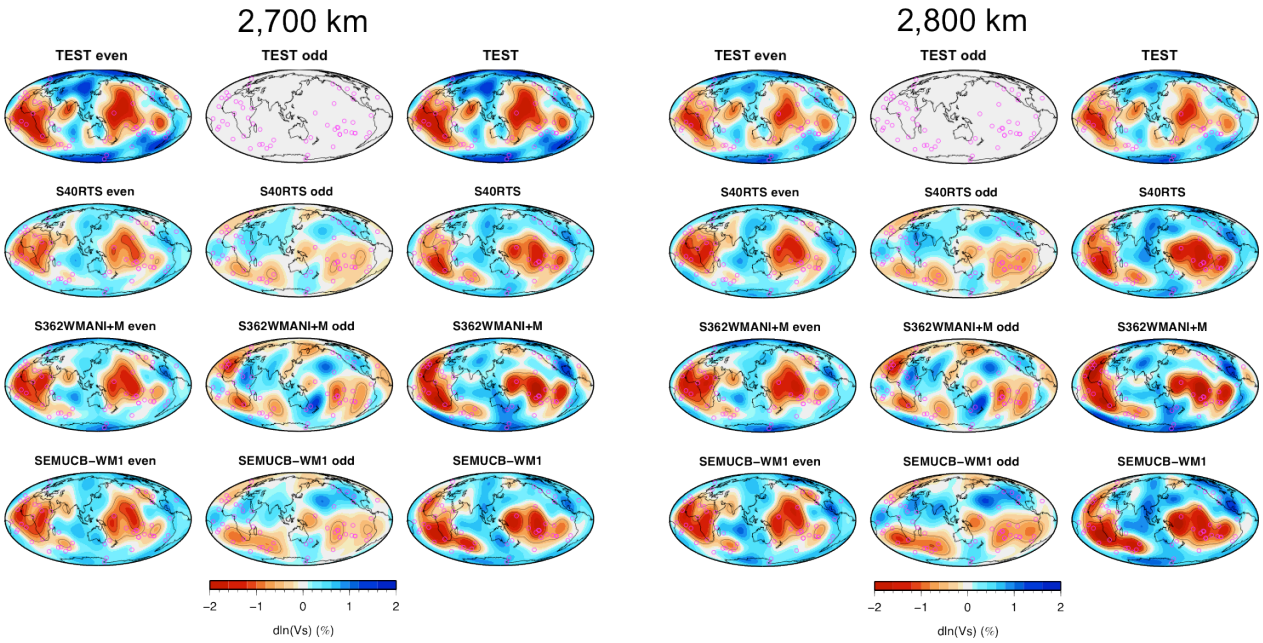

Figure 2. Even (left), odd (middle) and total tomographic models (right) displayed at 2,700 km (left) and 2,800 km (right) depths. For this test case we invert the same normal mode data as in S40RTS (top raw), the three other tomographic models are from *Ritsema et al.* [2011]; *Moulik & Ekström* [2014]; *French & Romanowicz* [2014] filtered up to the spherical harmonic degree 8 (2nd, 3rd and 4th raws). Since we include no cross-coupling data in this test case, the obtained model does not have any odd degrees at the base of the mantle. We can observe a very good agreement of the even part of SEISGLOB1 with the even part of the other models down to 2,800 km depth and no drastic change of the test model across D".

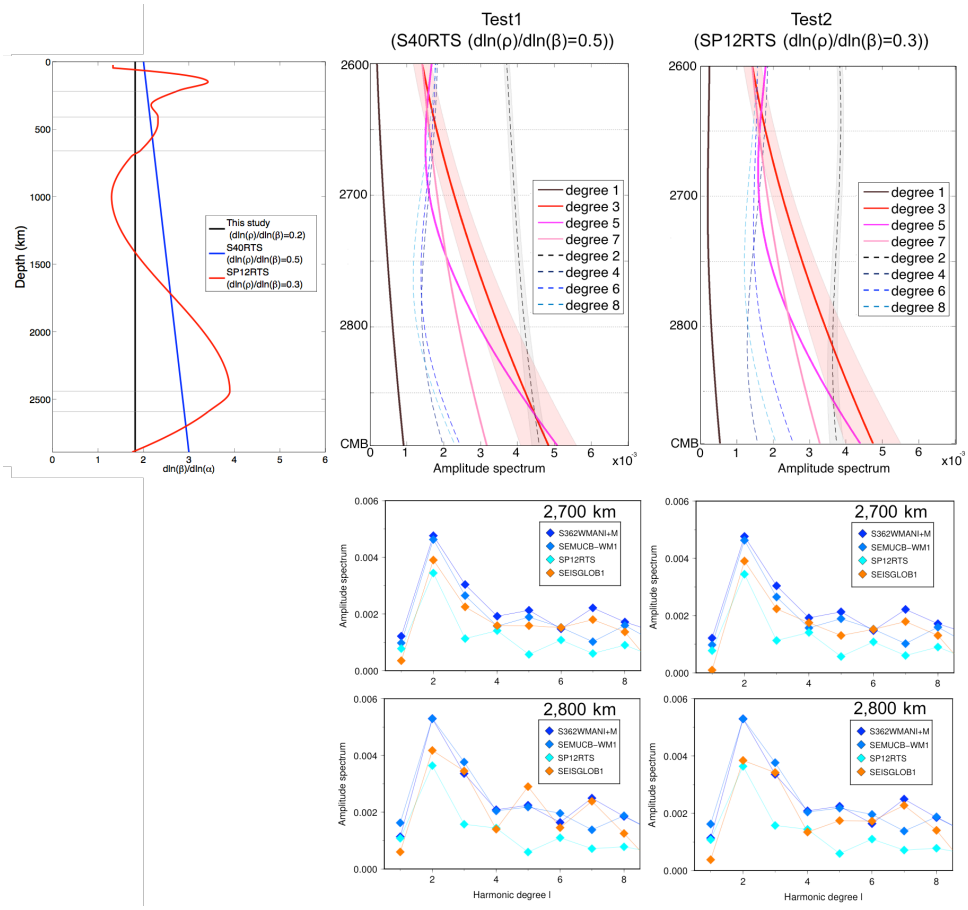

Figure 3. Left: (α,β) and (ρ,β) scalings used by this study (black), by *Ritsema et al.* [2011] (blue) and by *Koelemeijer et al.* [2016] (red). Middle column: Amplitude spectrum with depth (top panel) from 2,600 km depth down to the CMB for the tomographic model obtained using *Ritsema et al.* [2011] scaling laws (same as in S40RTS) and amplitude spectra at 2,700 (middle panel) and 2,800 km (bottom panel). Right column: Same as in middle column but using *Koelemeijer et al.* [2016] scaling laws (same as in SP12RTS). In both cases we observe an increase of the odd degrees with depth, with a degree 3 that is as large or greater than degree 2 at the CMB. Are also diplayed the *a posteriori* errors on degrees 2 and 3 (color shaded areas on top, middle and right panels) which show that our main result, that the odd/even degree amplitude ratio is larger than in previous model, is robust.

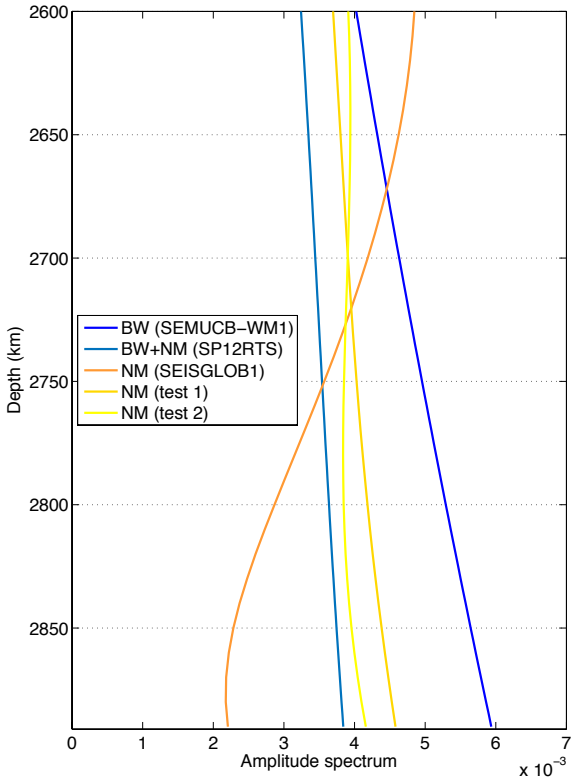

Figure 4. Amplitude of the degree 2 at the base of the mantle from various inversions: body wave data only (SEMUCB-WM1 [*French & Romanowicz*, 2014]), normal modes only (SEISGLOB1 and in two tests done with other (α,β) and (ρ,β) scaling laws) and a combination of normal modes and body waves (SP12RTS [*Koelemeijer et al.*, 2016]). BW denotes body waves and NM normal nodes. Test1 refers to the scaling used in S40RTS[*Ritsema et al.*, 2011] and Test2 to that deduced from SP12RTS [*Koelemeijer et al.*, 2016]. It really seems that the strong degree 2 seen by body waves (SEMUCB-WM1), is not required by normal modes.

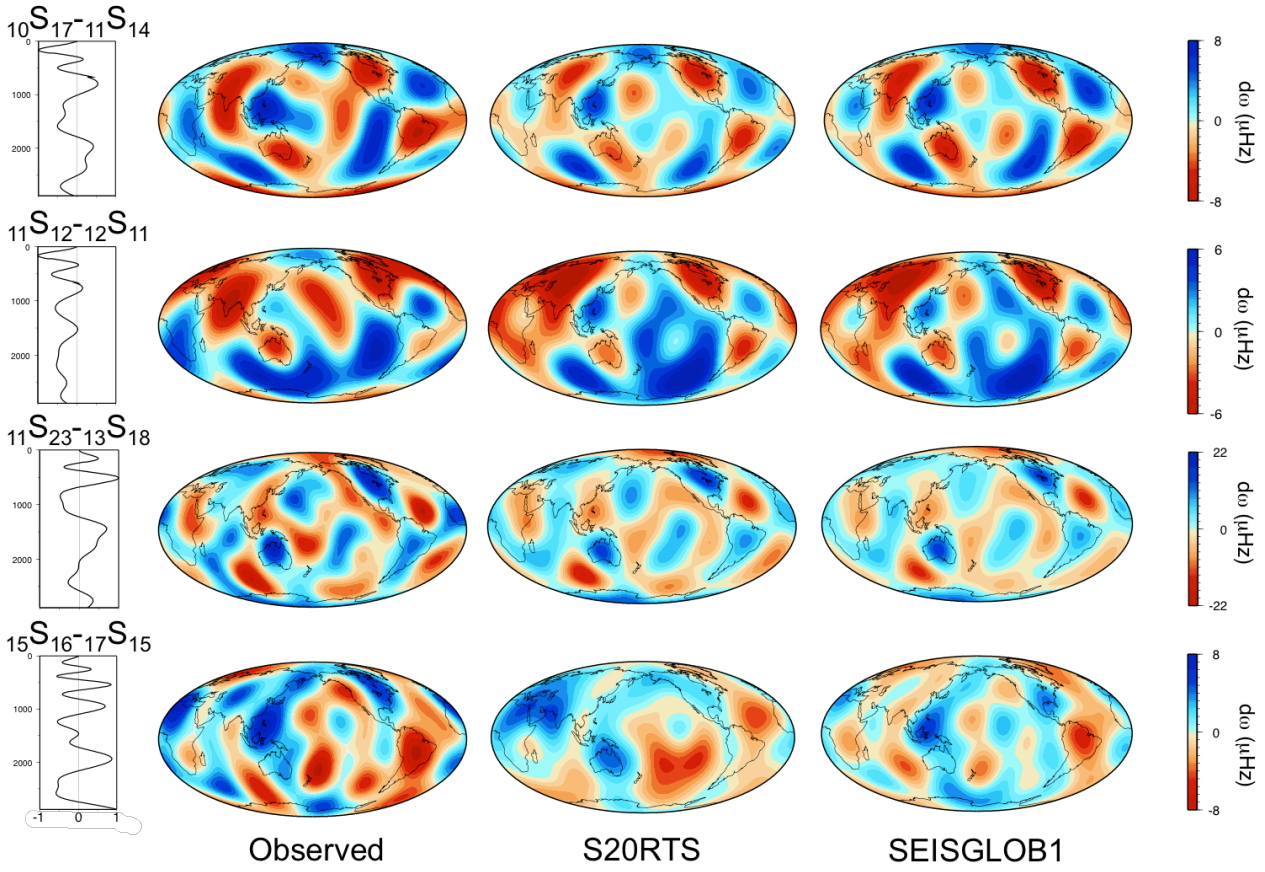

Figure 5. Observed (2nd column) and predicted (columns 3 and 4) splitting functions for the cross-coupling of the modes ${}_{10}S_{17}$-${}_{11}S_{14}$ (top row), ${}_{11}S_{12}$-${}_{12}S_{11}$ (2nd row), ${}_{11}S_{23}$-${}_{13}S_{18}$ (3rd row) and ${}_{15}S_{16}$-${}_{17}S_{15}$ (4th row). The observations have been computed from the measurements of *Deuss et al.* [2013] and the predictions have been computed for models SEISGLOB1 and S20RTS [*Ritsema et al.*, 2004]. In the first column are represented the corresponding normalized shear velocity kernels from the surface down to the CMB. Notice that for a mode where the kernel is rapidly varying through the D" layer (bottom row), SEISGLOB1 provides a much better fit to the observations.

Table 1. Self-coupling normal mode dataset used in the inversion (inner core sensitive modes have been excluded).

Branch	Modes
0	${}_0S_6 \cdots {}_0S_{60}$
1	${}_1S_2 \cdots {}_1S_{10}$, ${}_1S_{11} \cdots {}_1S_{16}$
2	${}_2S_4 \cdots {}_2S_{16}$, ${}_2S_{25}$
3	${}_3S_6 \cdots {}_3S_9$, ${}_3S_{25} \cdots {}_3S_{26}$
4	${}_4S_2 \cdots {}_4S_5$
5	${}_5S_3 \cdots {}_5S_8$, ${}_5S_{11}$-${}_5S_{12}$, ${}_5S_{14} \cdots {}_5S_{17}$
6	${}_6S_9 \cdots {}_6S_{10}$, ${}_6S_{15}$, ${}_6S_{18}$
7	${}_7S_5 \cdots {}_7S_9$
8	${}_8S_6 \cdots {}_8S_7$, ${}_8S_{10}$
9	${}_9S_8$, ${}_9S_{10} \cdots {}_9S_{15}$
10	${}_{10}S_{10}$, ${}_{10}S_{17} \cdots {}_{10}S_{21}$
11	${}_{11}S_9 \cdots {}_{11}S_{10}$, ${}_{11}S_{12}$, ${}_{11}S_{14}$, ${}_{11}S_{23} \cdots {}_{11}S_{25}$
12	${}_{12}S_6 \cdots {}_{12}S_7$, ${}_{12}S_{11} \cdots {}_{12}S_{17}$
13	${}_{13}S_{15} \cdots {}_{13}S_{16}$, ${}_{13}S_{18} \cdots {}_{13}S_{20}$
14	${}_{14}S_8 \cdots {}_{14}S_9$, ${}_{14}S_{14}$
15	${}_{15}S_{12}$, ${}_{15}S_{15} \cdots {}_{15}S_{16}$
16	${}_{16}S_{10} \cdots {}_{16}S_{11}$, ${}_{16}S_{14}$
17	${}_{17}S_{12} \cdots {}_{17}S_{15}$
18	-
19	${}_{19}S_{10} \cdots {}_{19}S_{11}$

Table 2. Cross-coupling normal mode dataset used in the inversion (inner core sensitive modes have been excluded).

Branch	Modes
0	${}_0S_{11}$-${}_2S_7$, ${}_0S_{14}$-${}_2S_9$, ${}_0S_{17}$-${}_2S_{11}$
1	${}_1S_3$-${}_3S_1$
2	${}_2S_8$-${}_4S_3$, ${}_2S_7$-${}_5S_5$, ${}_2S_{10}$-${}_4S_5$
3	${}_3S_7$-${}_5S_5$, ${}_3S_8$-${}_6S_3$
4	-
5	${}_5S_{14}$-${}_9S_8$, ${}_5S_{16}$-${}_8S_{10}$
6	${}_6S_{15}$-${}_9S_{10}$
7	${}_7S_8$-${}_5S_{11}$, ${}_7S_6$-${}_6S_9$
8	-
9	${}_9S_6$-${}_7S_9$, ${}_9S_{12}$-${}_{10}S_{10}$, ${}_9S_{14}$-${}_{14}S_7$, ${}_9S_{15}$-${}_{14}S_8$
10	${}_{10}S_{17}$-${}_{11}S_{14}$, ${}_{10}S_{21}$-${}_{12}S_{16}$
11	${}_{11}S_{12}$-${}_{12}S_{11}$, ${}_{11}S_{23}$-${}_{13}S_{18}$
12	${}_{12}S_{12}$-${}_{16}S_7$
13	-
14	${}_{14}S_{13}$-${}_{16}S_{11}$
15	${}_{15}S_{16}$-${}_{17}S_{15}$
16	-
17	${}_{17}S_{12}$-${}_{21}S_7$

Table 3. Description of the different tomographic models used in this study.

Models	Horizontal	Vertical	Radial	Data	Theory
S362WM ANI+M	spheric. splines	16 cubic splines discontinuous across 650 km	y	Long period body wave waveforms, body wave travel time delays, surf. wave phase velocity normal mode self-coupling coeff.	Ray theory
SP12RTS	Spheric. harm. up to degree 12	21 splines spacing increasing with depth	n	Body wave travel time delays, Fundamental & overtones surf. waves normal mode self-coupling coeff., including Stoneley modes	Ray theory
SEMUCB -WM1	Spheric. splines	20 cubic b-splines	y	Fundamental & overtones surf. waves waveforms (T > 60 s), body wave waveforms (T > 36 s and T > 32 s)	3D synthetics and NACT
SEISGLOB1	Spheric. harm. up to degree 20	21 splines, spacing increasing with depth	n	Fundamental & overtones surf. waves and normal mode self- and cross-coupling coeff.	Ray theory

Table 4. Data misfit obtained for the modes presented in Figure 4 for the inversions done with the two other scaling laws presented in Supplementary Figure S1. Test1 refers to the scaling used in S40RTS[*Ritsema et al.*, 2011] and Test2 to that used in SP12RTS [*Koelemeijer et al.*, 2016]. The misfits are very similar except for the Stoneley mode ${}_1S_{13}$ for which our depth independent scaling performs better.

Models	${}_6S_{15}$-${}_9S_{10}$	${}_9S_6$-${}_7S_9$	${}_{12}S_{12}$-${}_{16}S_7$	${}_{15}S_{16}$-${}_{17}S_{15}$	${}_{11}S_{10}$	${}_{13}S_{16}$	${}_1S_{13}$	${}_2S_{25}$
SEISGLOB1	0.18	0.64	0.82	0.64	0.37	0.33	0.14	0.19
Test1	0.17	0.66	0.85	0.60	0.34	0.32	0.26	0.16
Test2	0.19	0.62	0.85	0.66	0.33	0.31	0.25	0.18

Table 5. Normal mode data misfit computed for SEISGLOB1 and various tomographic models. For each mode i, the misfit is defined as $M_i = \sqrt{\sum_{st}\left[\left(c^t_{s,synth} - c^t_{s,obs}\right)^2\right] / \sum_{st}\left[\left(c^t_{s,obs}\right)^2\right]}$ where s and t are respectively the spherical harmonic degrees and orders, $c^t_{s,obs}$ are the measured coefficients, and $c^t_{s,synth}$ the coefficients computed in a given tomographic models. The average misfit M is defined as $\sqrt{1/N \sum_i^N M_i^2}$ where N is the number of modes. We present in colunm "odd" the average misfit for every mode constraining the odd degrees of the mantle structure, so actually only cross-coupling data ; in column "even" the average misfit for every modes constraining the even degrees so including self-coupling data and some cross-coupling data ; in column "Stoneley modes" the average misfit for the self-coupling of Stoneley modes only. Test1 refers to the inversion using the scaling of S40RTS[*Ritsema et al.*, 2011], Test2 that from SP12RTS [*Koelemeijer et al.*, 2016]). Table 1 shows that SEISGLOB1 better explains the mode data that previous models. The depth-dependent scalings of Test1 and Test2 do not yield a significantly better fit.

Models	odd (s=1,3,5,7)	even (s=2,4,6,8)	Stoneley modes (s=2,4,6,8)	total
SEISGLOB1	0.54	0.41	0.19	0.42
Test1	0.55	0.41	0.20	0.42
Test2	0.55	0.39	0.19	0.40
SEMUCB-WM1	0.90	0.69	0.32	0.70
S362WMANI+M	1.02	0.77	0.30	0.79
SP12RTS	0.77	0.65	0.25	0.66